Wiggling Error Self-Calibration for Indirect ToF Image Sensors

Min-Sun Keel, Daeyun Kim, Jiheon Park, Sooho Son, Bumsik Chung, Jonghan Ahn, Yeomyung Kim, Myunghan Bae, Hoyong Lee, Myoungoh Ki, Myeonggyun Kye, Il-pyeong Hwang, Seung-chul Shin, Young-Gu Jin, Youngsun Oh, Yitae Kim, Jesuk Lee and Duckhyun Chang

System LSI Division, Samsung Electronics Co., Ltd., Hwaseong, Gyeonggi-do, Korea,
Phone: +82-31-8037-2017, E-mail: ms.keel@samsung.com

Abstract — We propose a method to self-calibrate wiggling distance error in the indirect time-of-flight (ToF) image sensor system. The basic idea is to minimize harmonic components in the demodulation signals by equivalent waveform shaping. During the exposure time, demodulation signals are phase-shifted gradually at every demodulation pulse cycle up to a specific phase delay, to emulate sinusoid signals with the smallest harmonics. The proposed phase delay control circuit was implemented in the 1.2-Mpixel indirect ToF sensor. The optimal phase delay is found by the simulation and verified by the measurement results. The proposed wiggling self-calibration achieved a distance error of less than 4 mm with an optimal phase delay of 123°, which is about 12 times smaller than that of the uncalibrated case.

I. Introduction

Time-of-flight (ToF) image sensors are gaining popularity to obtain three-dimensional (3-D) depth maps with relatively simple hardware. To improve depth accuracy and stability, specific calibration steps are required. The common calibration items are temperature, global offset, fixed-pattern phase noise (FPPN), and wiggling distance error. The wiggling distance error, or cyclic error, is a depth distortion with a cyclic pattern, which is periodic with the distance [1]. To cancel out wiggling error by gathering data from different distances, there are several approaches such as 1) physical position movement of a flat chart, 2) optical fibers with different lengths, and 3) electrical delay injection between the illuminator and the sensor. All the above methods require space, time, and cost, which is undesirable for mass production.

In this paper, we present a self-calibration scheme for wiggling error in the indirect ToF systems, so that the calibration step for wiggling error is not required. Wiggling errors originate from harmonic component aliasing into a fundamental frequency when both modulation and demodulation signals have harmonic components [1], [2]. To minimize wiggling error, harmonic rejection at the modulation signal was proposed in [2]. However, the work in [2] needs exact exposure time control, which is not possible when auto-exposure (AE) is applied. Our proposed idea can solve this issue by simple timing control.

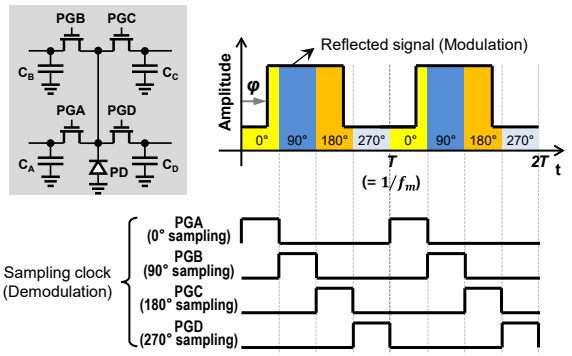

Fig. 1. Modulation and demodulation signals for 4-phase sampling in a 4-tap demodulation pixel. Timing diagram and partial schematic of the 4-tap demodulation pixel are shown.

II. Basic Theory

Fig. 1 shows typical waveforms for the modulation and demodulation signals in an indirect ToF system with a 4-tap demodulation pixel [3]. The modulation signal is a continuous-wave periodic signal with a period of $T = 1/f_m$ (f_m: modulation frequency). The phase shift (φ) can be calculated by the four-phase sampling [4], which can be determined as follows for a 4-tap pixel if sinusoid modulation is assumed:

$$\varphi = \operatorname{atan}\left[\frac{A_1 - A_3}{A_0 - A_2}\right] - \frac{\pi}{4}, \qquad (1)$$

where A_0, A_1, A_2, and A_3 are the sampled signals, or cross-correlation signals at 0°, 90°, 180°, and 270° phase points, respectively, and the phase offset of $\pi/4$ can be removed by the global offset calibration. To gather all four sampled data in a frame, a 4-tap pixel is used, which is advantageous for lower motion artifacts [3]. The 4-tap pixel has four storage capacitors (C_A, C_B, C_C, and C_D) and four photo-gates (PGA, PGB, PGC, and PGD), as shown in the inset of Fig. 1 for a simplified pixel; the photo-gates are controlled by sampling clocks with 25% duty-cycle (see the timing diagram at the bottom of Fig. 1).

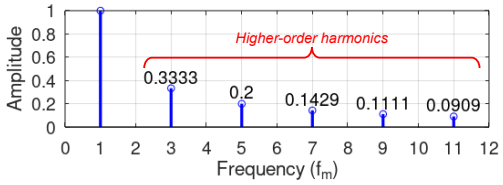

Fig. 2. Frequency domain representation of a rectangular modulation signal with harmonic components.

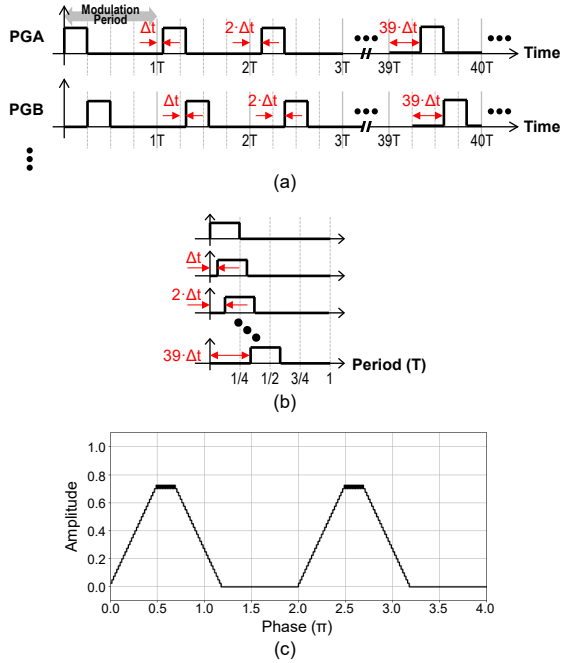

Fig. 3. The proposed wiggling error self-calibration. (a) Demodulation signal manipulation with delay control (only PGA and PGB are shown for simplicity). (b) Demodulation pulse, redrawn at each cycle for better understanding. (c) Equivalent demodulation signal with 120° phase delay.

In practice, for easier implementation, modulation and demodulation signals are implemented by rectangular pulses, which have higher-order harmonic components at every odd multiple of the fundamental frequency, as shown in Fig. 2 using the Fourier series analysis [2]. In four-phase sampling, the odd harmonics will be aliased into the fundamental frequency, which will distort the φ value in (1).

III. Proposed Scheme

The underlying concept of our proposed wiggling error self-calibration is based on the harmonic rejection mixer in [5]. The rectangular pulse stream for demodulation will be equivalently reshaped into the sinusoid-like signal by the optimal delay control. The work in [2] also adopted a similar concept at the modulation signal. However, [2] requires exposure time control with a ratio of irrational numbers such as $\sqrt{2}$ or $\sqrt{3}$, which complicates proper exposure time calculation during AE operation.

Fig. 3(a) shows the timing diagram of our proposed method; part of exposure time is magnified, and only

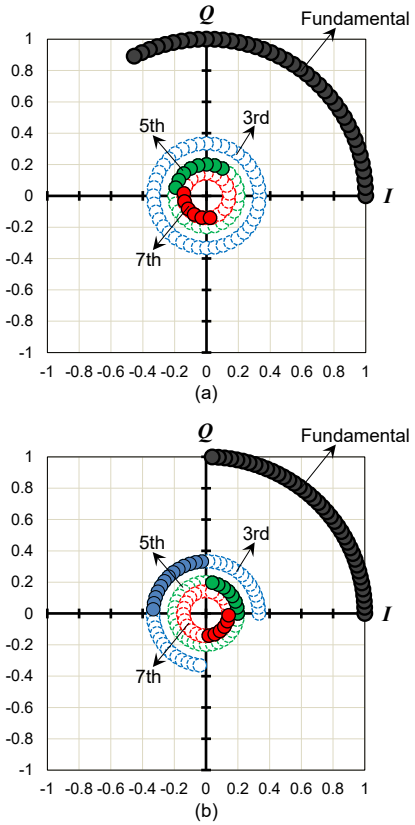

Fig. 4. Explanation of harmonic rejection on a complex plane (dots with 360° turns are colored as white). (a) 120° phase delay (optimal for wiggling error minimization). (b) 90° phase delay (optimal for peak current reduction).

two out of the four demodulation signals are shown for simplicity. The initial phase of each demodulation pulse cycle with a duration of T is gradually delayed by accumulating a unit time delay (Δt), up to 40 cycles, and this operation repeats by the end of the exposure time. For f_m = 100 MHz, the complete 40-cycle will take only 400 ns, which is a fine step for a good AE control. Fig. 3(b) redraws Fig. 3(a) by aligning each demodulation cycle for better understanding. With the proposed demodulation delay control, the equivalent demodulation signal is reshaped into a trapezoidal pulse, as plotted in Fig. 3(c) with a 120° phase delay, as an example.

The proposed harmonic rejection mechanism can be explained on a complex plane, as shown in Fig. 4; the fundamental, 3rd, 5th, and 7th harmonics are plotted as colored dots, with the dots of complete 360° turn colored in white. Theoretically, when the total phase delay is 120°, all 3rd harmonic vectors are canceled by making a complete 360° turn on the complex plane, and the other components such as 5th and 7th harmonics are minimized, as illustrated in Fig. 4(a). Hence, wiggling error is expected to be minimal around 120° phase delay. For comparison, the phase delay of 90° is also plotted in Fig. 4(b); all higher-order harmonics still remained. However, 90° phase delay is beneficial to peak current reduction, when combined with the multiple-interleaving scheme in [3].

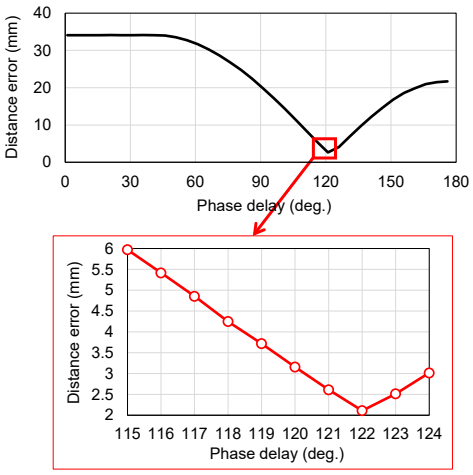

Fig. 5. Wiggling error simulation results with the phase delay at f_m = 100 MHz. The phase delay of 122° gives the most optimal result with the smallest distance error.

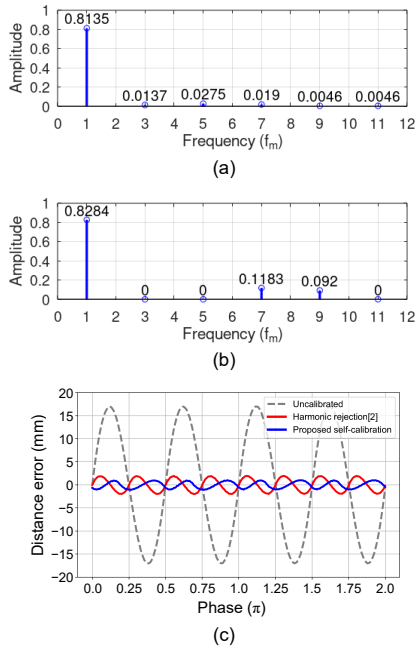

Fig. 6. Simulation results for harmonic rejection. (a) Proposed self-calibration with a phase delay of 122°. (b) Harmonic rejection in [2]. (c) Distance error comparison at f_m = 100 MHz.

The harmonic rejection effect from the proposed method is verified by simulation; the optimal phase delay for the minimal wiggling error can be found. Fig. 5 shows the simulation results of distance error with a phase delay. Distance error is defined as the difference between the maximum and minimum distance offsets from the ground truth. Fig. 5 shows a notch around 120° phase delay, as expected in Fig. 4. The minimum distance error occurs at the 122° phase delay.

In the frequency domain plots for the harmonic components, our proposed method at the 122° phase delay in Fig. 6(a) is compared to that of [2] in Fig. 6(b). For a minimal wiggling error, the summation of amplitudes of all harmonic components should be minimized. The harmonic rejection in [2] can

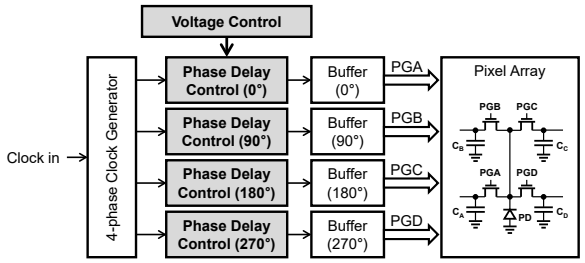

Fig. 7. Circuit block diagram for the proposed wiggling self-calibration.

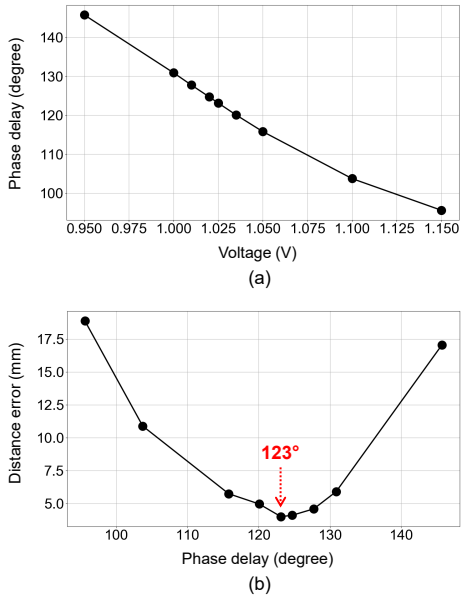

Fig. 8. (a) Measured phase delay vs. control voltage, and (b) distance error vs. phase delay (f_m = 100 MHz).

completely remove 3rd and 5th harmonic components. However, the aggregate harmonic amplitude of our proposed scheme is smaller than that of [2] (compare Fig. 6(a) to (b)). Fig. 6(c) shows wiggling errors from different cases at the 100-MHz modulation frequency. Without any calibration ("uncalibrated"), wiggling error is as large as 34.02 mm. With our proposed method, the error can be reduced to 2.1 mm, whereas harmonic rejection in [2] decreases error to 3.94 mm. Thus, the proposed scheme can provide better wiggling error cancellation by 47% error reduction compared to the prior work in [2].

IV. Hardware Implementation and Measurement Results

The proposed scheme is implemented as a part of the 1.2-Mpixel indirect ToF sensor chip in [3]. The simplified circuit block diagram is presented in Fig. 7. The 4-phase clock generator produces four demodulation clocks. The phase delay control block generates the unit time delay (Δt) as introduced in Fig. 3(a) and accumulates it to determine the total phase delay ($40\times\Delta t$). The Δt value is tuned by a supply voltage, which is controlled by the internal voltage regulator or external supply.

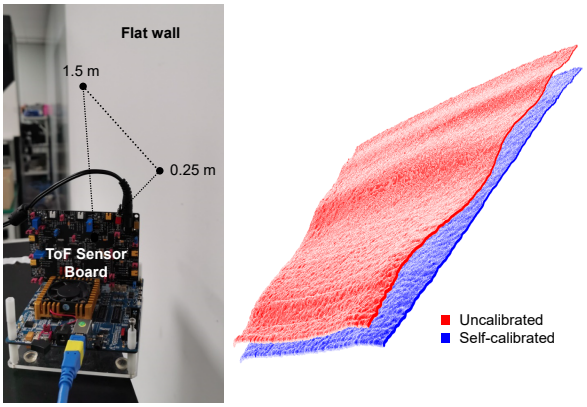

Fig. 9. Depth map comparison of a flat wall with f_m = 100 MHz (1.5-m unambiguous range). (a) Test set-up. (b) 3-D point cloud comparison between uncalibrated and self-calibrated cases.

Fig. 8 shows the measurement results of the phase delay and wiggling error. Fig. 8(a) shows the measured phase delay according to the control voltage. Fig. 8(b) is a measured wiggling error with the phase delay. The minimum error is obtained at the phase delay of 123° from 1.025 V control voltage, which almost conforms to the simulation result in Fig. 5.

Fig. 9 shows the measurement set-up and 3-D point clouds of a flat wall, to show the performance of the proposed scheme. The ToF sensor is capturing the flat wall at a tilt angle to take depth data from the 0.25 m to 1.5 m distance in a single depth map (see Fig. 9(a)). As shown in Fig. 9(b), the proposed self-calibration scheme shows a much flatter depth map (blue), compared to the uncalibrated one (red).

The measured cross-correlations, A_0 to A_3, are plotted in Fig. 10(a) and (b) for the uncalibrated and the self-calibrated cases, respectively. For the uncalibrated case, rectangular pulses are used both for the modulation and demodulation processes. Thus, the cross-correlation functions are isosceles trapezoidal shapes, as shown in Fig. 10(a). And as these functions are approximated as sinusoids to calculate φ in (1), wiggling error occurs. However, with the proposed scheme, the shape of the cross-correlation functions is more like a sinusoid as shown in Fig. 10(b), which can minimize wiggling error.

Fig. 11 compares the measured wiggling error between the uncalibrated and self-calibrated schemes. The uncalibrated case shows a wiggling error of 49.3 mm, whereas the proposed self-calibration reduces the error to less than 4 mm, which is more than 12× improved and sufficiently small to exclude the wiggling calibration.

V. Conclusion

A novel method to remove the wiggling calibration was proposed. By accumulating optimal time delay, the harmonic components in the demodulation signals can be minimized, which reduces wiggling error. The time delay can be tuned by the control voltage of the phase delay control block. From the simulation and measurement results, the optimal phase delay was identified, and wiggling error could be improved by more than 12 times, compared to the uncalibrated case. With the proposed scheme, one of the tedious and expensive calibration steps, the wiggling calibration, can be ignored, to reduce overall ToF camera cost.

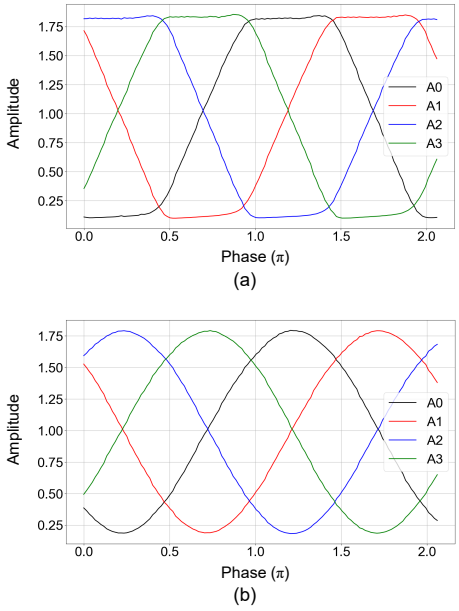

Fig. 10. Cross-correlation plots. (a) Uncalibrated, and (b) self-calibrated cases.

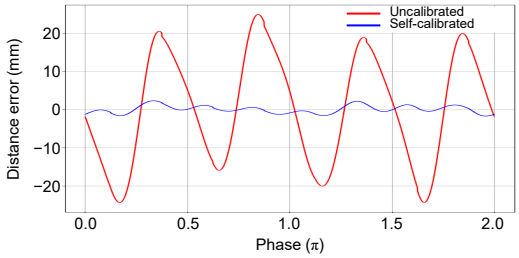

Fig. 11. Distance error comparison. (a) Uncalibrated, and (b) self-calibrated cases (f_m = 100 MHz).

References

[1] S. Foix *et al.*, "Lock-in Time-of-Flight (ToF) Cameras: A Survey," *IEEE Sensors Journal*, vol. 11, no. 3, Mar. 2011.

[2] A. D. Payne *et al.*, "Improved linearity using harmonic error rejection in a full-field range imaging system," *Proc. SPIE*, vol. 6805, 2008.

[3] M. S. Keel *et al.*, "A 4-tap 3.5μm 1.2Mpixel Indirect Time-of-Flight CMOS Image Sensor with Peak Current Mitigation and Multi-User Interference Cancellation," *ISSCC Dig. Tech. Papers*, pp. 106-108, Feb. 2021.

[4] R. Lange and P. Seitz, "Solid-state time-of-flight range camera," *IEEE J. Quantum Electron.*, vol. 37, no. 3, pp. 390-397, Mar. 2001.

[5] J. A. Weldon *et al.*, "A 1.75-GHz highly integrated narrow-band CMOS transmitter with harmonic-rejection mixers," *IEEE JSSC*, vol. 36, pp. 2003-2015, 2001.